14th World Congress in Computational Mechanics (WCCM)
ECCOMAS Congress 2020
Virtual Congress: 11 – 15 January 2021
F. Chinesta, R. Abgrall, O. Allix and M. Kaliske (Eds)

MICROMECHANICAL ANALYSIS OF DETACHMENT MECHANSIMS OF SUFFUSION

QIRUI MA[1] [2] , ANTOINE WAUTIER[2] AND WEI ZHOU[1]

[1] School of Water Resources and Hydropower Engineering, Wuhan University
8 Donghu South Road, 430072 Wuhan, China

[2] INRAE, Aix-Marseille University, UR RECOVER,
3275 Route Cézanne, CS 40061, Aix-en-Provence, France

*qirui.ma@inrae.fr

Abstract: Suffusion is a typical phenomenon of seepage-induced internal erosion, corresponding to fine particles erosion from the coarse matrix under the action of a fluid. A three-dimensional and spatially resolved fluid-solid coupling method based on lattice Boltzmann method (LBM) and discrete element method (DEM) is proposed to simulate suffusion in binary mixtures under anisotropic stress states. Based on such numerical simulations, eroded grains are identified and the mean squared displacement as well as the ratio between drag force and contact force of these eroded particles are computed to describe the detachment mechanism. The results show that the fluid force acting on eroded particles increases in the simulation which corresponding to the steep slope in squared displacements. Regardless of the initial state, the ratio between the fluid force and the contact force of the eroded particles displays a downward trend over time, reflecting the gradual dominance of the fluid force, which eventually leads to particle detachment and erosion. Based on the judgment between the direction of the fluid force and the direction of the contact force, a contact index P is then proposed to determine whether the contact is going to slide or strengthen under the action of the fluid. The distribution of indexes P for the contacts of eroded particles just prior to their detachment reflects that fluid induced sliding dominates. A particle detachment index is thus proposed and the overall detachment sensitivity of the binary samples is eventually investigated with respect to the fluid flow direction.

Key words: Granular Materials, Suffusion, DEM, LBM, Particle Detachment.

1 INTRODUCTION

Suffusion is a typical form of internal erosion, which can be described as the phenomenon of finest particle detach, transport and migrate in the void of structure formed by coarse particle. In geotechnical engineering, 46% of the earth rock dam damage is originated from internal erosion according to the recorded statistics[1][2]. Extensive experimental tests have been carried out to study internal stability and critical hydraulic gradient in internal erosion [3][4][5][6].

However, some research have found that the soil strength of corroded specimens is weakened [7], but others have found that the corroded specimens have stronger liquefaction resistance under cyclic shear [8][9]. This means the influence of suffusion on soil has not been fully understood. However, due to the limitation of physical experiment conditions, micro mechanism cannot be well interpreted, so DEM (Discrete element method) provides a solution to simulate the suffusion from grain level[10]. Some researchers have already used unresolved CFD (computational fluid dynamic)-DEM coupling method to study the suffusion[11][12][13]. Compared with unresolved CFD-DEM, LBM (lattice Boltzmann method)-DEM coupling method, which can capture the details of fluid/grain interaction better, it is rare to carry out the research of suffusion. Moreover, many studies have not explored the process of particle detachment and clogging, but more focused on the final results. But the fully understanding of the particle detachment and migration in the microscale is essential to expound the occurrence of suffusion Therefore, in this paper, LBM-DEM method is used to simulate the mechanism of particle detachment in the suffusion process.

2 SIMULATION PROCESS

2.1 Method

The three-dimensional LBM-DEM coupling method based on two open-source software, LIGGGHTS responsible for the solid part in DEM [11], Palabos solve the fluid region in LBM [14]. As for the fluid/grain coupling part, the immersed moving boundary is selected to solve the interaction between solid and fluid[15]. The detail of the coupling method will be briefly introduced respectively.

In LBM, the governing formula can be written as[16],

$$f_i(\mathbf{x}+\mathbf{c}_i\delta_t, t+\delta_t) - f_i(\mathbf{x},t) = -\frac{1}{\tau}\left[f_i(\mathbf{x},t) - f_i^{eq}(\mathbf{x},t)\right] \tag{1}$$

where the f_i is denotes the density distribution function whose coordinate is $\mathbf{x}$ directing in the *i*-th path at time *t*; $\mathbf{c}_i$ represents 19 discrete velocity vectors, because the D3Q19 LBM model is used in this study ; and τ is a relaxation coefficient, which controls the stability of LBM simulation. The equilibrium distribution functions $f_i^{eq}(\mathbf{x},t)$ in the right side of Eq. (1) is defined as,

$$f_i^{eq} = w_i \rho_{\text{fluid}} \left[1 + \frac{\mathbf{c}_i \cdot \mathbf{u}_{\text{fluid}}}{c_s^2} + \frac{(\mathbf{c}_i \cdot \mathbf{u}_{\text{fluid}})^2}{2c_s^4} - \frac{|\mathbf{u}_{\text{fluid}}|^2}{2c_s^2} \right] \quad (i = 0,...,18) \tag{2}$$

Where $w_i\,(i=0,...,18)$ are the weighting factors, w_0=1/3, $w_{1\text{-}6}$ =1/18, $w_{7\text{-}18}$ =1/36 ; ρ_{fluid} and $\mathbf{u}_{\text{fluid}}$ are the density and velocity of fluid, respectively. The sound speed c_s =1/3 in the lattice units in the 3D LBM model [17].

According to the transfer method, the fluid velocity, fluid density, and fluid pressure in the macroscopic scale can be calculated through LBM quantities as follows[18][19]:

$$\rho_{\text{fluid}} = \sum_{i=0}^{18} f_i \tag{3}$$

$$\mathbf{u}_{\text{fluid}} = \frac{1}{\rho_{\text{fluid}}} \sum_{i=0}^{18} \mathbf{c}_i f_i \tag{4}$$

$$p_{\text{fluid}} = c_s^2 \rho_{\text{fluid}} \tag{5}$$

In DEM, the spherical particles' displacement is controlled by the Newton's second law of motion [10]:

$$m_i \mathbf{a} = \mathbf{F}_c + \mathbf{F}_{\text{fluid}} \tag{6}$$

$$I_i \dot{\boldsymbol{\omega}} = \mathbf{T}_c + \mathbf{T}_{\text{fluid}} \tag{7}$$

where I_i is the moment of inertia of particle, m_i is the mass of the particle; $\mathbf{a}$ is the motion acceleration; $\boldsymbol{\omega}$ is the angular velocity; $\mathbf{F}_c$ are the contact forces between particles and $\mathbf{T}_c$ is corresponding torques provided by particle collision; $\mathbf{F}_{\text{fluid}}$ and $\mathbf{T}_{\text{fluid}}$ are the hydrodynamic force and the corresponding torque provided by the fluid part, respectively. The normal force $\mathbf{F}_n$ and tangential force $\mathbf{F}_t$ between two particles are calculated by the Hertz-Mindlin contact model.

Fluid-solid interaction calculations are achieved by adding a collision term Ω_i^s to Eq. (1), the govern equation becomes

$$f_i(\mathbf{x} + \mathbf{c}_i \delta_t, t + \delta_t) - f_i(\mathbf{x}, t) = -\frac{1}{\tau}\left[f_i(\mathbf{x}, t) - f_i^{\text{eq}}(\mathbf{x}, t)\right](1 - B) + B\Omega_i^s \Big] \tag{8}$$

$$\Omega_i^s = f_{-i}(\mathbf{x}, t) - f_{-i}^{\text{eq}}(\rho_{\text{fluid}}, \mathbf{u}_{\text{fluid}}) + f_i^{\text{eq}}(\rho_{\text{fluid}}, \mathbf{u}_s) - f_i(\mathbf{x}, t) \tag{9}$$

where $B = \dfrac{\varepsilon(\tau - 0.5)}{(1-\varepsilon) + (\tau - 0.5)}$, which is a weighting function of relaxation coefficient τ and solid ratio ε of the LBM cell. $\varepsilon = V_{\text{solid}} / V_{\text{cell}}$, and thus, ε = 0(1) yields B = 0(1). The subscript -*i* in the Eq. (9) represents the opposite direction of *i*.

Taking the effect of grain rotation into consideration, the velocity of the solid part $\mathbf{u}_s$ is calculated as [20],

$$\mathbf{u}_s = \mathbf{u}_p + \boldsymbol{\omega}_p \times \left[\left(\mathbf{x} + 0.5\mathbf{c}_i \delta_t \right) - \mathbf{x}_p \right] \tag{10}$$

where $\mathbf{u}_p$ and $\boldsymbol{\omega}_p$ are translational and angular velocities of solid grain, and $\mathbf{x}_p$ is the position of solid grain.

Lastly, the hydrodynamic force $\mathbf{F}_{\text{fluid}}$ and the corresponding hydraulic torque $\mathbf{T}_{\text{fluid}}$ applied by fluid motion can be calculated as:

$$\mathbf{F}_{\text{fluid}} = \sum_{j=1}^{n} B_j \sum_{i=0}^{18} \Omega_i^s \mathbf{c}_i \tag{11}$$

$$\mathbf{T}_{\text{fluid}} = \sum_{j=1}^{n} \left[B_j (\mathbf{x}_j - \mathbf{x}_p) \times \sum_{i=0}^{18} \Omega_i^s \mathbf{c}_i \right] \tag{12}$$

Where n is the total number of lattice cells covered by the solid part; B_j refer to the weight coverage function in j-th lattice cell among n lattice cells.

2.2 Suffusion simulation

The numerical simulation takes macroscopic fluid direction, hydraulic gradient, and vertical stress levels as factors to conduct research. The schematic figure of the simulation is shown in Fig. 1.

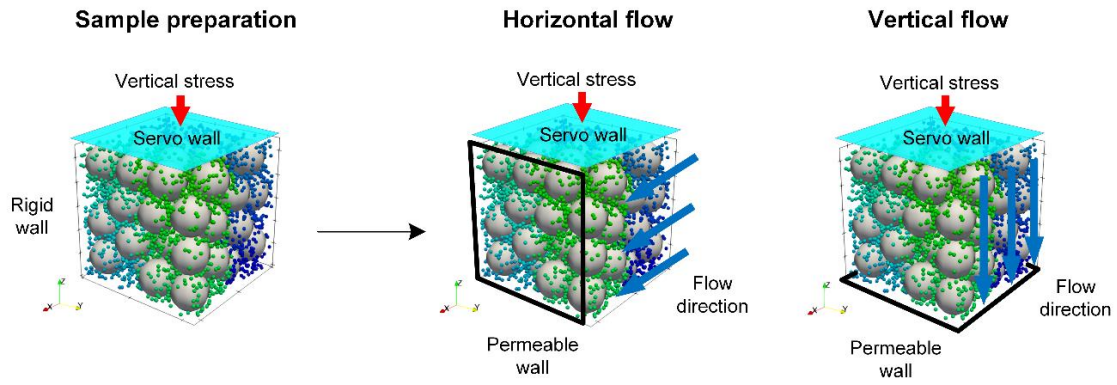

Fig.1 Suffusion simulations consider different flow direction

The binary packing consisting of only two types of particles with a particle size radius ratio of 10. The fines content (FC) of binary mixture are critical to sample's mechanical behavior. In this paper, FC is set to 30% which is in the transition region between "underfilled" and "overfilled"[21][3].

A binary packing with 26,788 particles is randomly inserted in the box firstly, then radius explosion method is adapted to achieve the target radius. After applying 100 kPa in the boundary for consolidation, a prepared binary mixture with dimension 0.11×0.11×0.11 m is obtained. For the sake of preventing boundary effect, the subsequent analysis is only based on the central volume (0.10×0.10×0.10 m). Then, the binary packing is compressed vertically to prescribed stress levels with a servo-controlled method in the top boundary, while rigid wall is applied in confining direction and bottom (this results in anisotropic stress state). When the equilibrium of the sample is reached under prescribed compressive stress, it will be considered as the end of sample preparation and the beginning of suffusion simulation.

Apply a hydraulic gradient in the direction of flow to generate fluid force to simulate particle erosion. In the flow direction (x-axis in the horizontal flow, z-axis in the vertical flow), the fluid pressure drop Δp applied on the upstream and downstream is based on the hydraulic gradient I ($\Delta p=\rho ghI$). Zero flux conditions are imposed in other directions. Permeable wall in the flow direction is taken place of the rigid wall as the suffusion simulation begins. Therefore, small particles are accessible to eroded form the sample by pass through the permeable wall. The values of the hydraulic gradient considered in this study are 0.1 and 1.0, and the values of the vertical stress levels are 0.1 MPa and 0.5 MPa. They are summarized in Table 1. The detailed parameters used in DEM and LBM simulations are summarized in Table 2.

Table 1 The simulations carried out based on various conditions

Conditions	Vertical stress, σ_v (MPa)	Stress ratio, η	Hydraulic gradient, I	Flow direction
Case 1	0.1	0.7	1.0	Horizontal
Case 2	0.5	1.1	0.1	Horizontal
Case 3	0.5	1.1	1.0	Horizontal
Case 4	0.5	1.1	1.0	Vertical
Case 5	0.1	0.7	-	-
Case 6	0.5	1.1	-	-

Table 2 Parameters of the LBM-DEM simulations

	Parameters	Units	Values
DEM	Particle density, ρ	kg/m^3	2600
	Particle number, N_{total}		26788
	Contact model		Hertz-Mindlin
	Young's module, Y	GPa	25
	Poisson ratio, v		0.3
	Maximum diameter, d_{max}	mm	30
	Minimum diameter, d_{min}	mm	3
	Particle size ratio		10
	Sliding friction, μ		0.5
	Rolling friction, μ_r		0.1
	DEM timestep, Δt_{DEM}	s	4.45×10^{-8}
LBM	Fluid density, ρ_{fluid}	kg/m^3	1000
	Kinematic viscosity, v_{fluid}	m^2/s	1.01×10^{-6}
	LBM timestep, Δt_{LBM}	s	4.45×10^{-7}

3 RESULTS AND DISCUSSIONS

The fluid forces experienced by a few particular eroded particles during suffusion process are shown in Figure 2a. In order to figure out the time dependence of displacement from the view of a single erosive particle, the variation of the translational mean squared displacement (TMSD) of these particles is also analyzed. The TMSD is calculated by the following equation:

$$\left\langle d^2(t)\right\rangle = \left\langle \left| r_j(t) - r_j(0) \right|^2 \right\rangle \tag{13}$$

where $r_j(t)$ is the position of particle j at time t. Figure 2b describes the distribution of the TMSD in horizontal flow with vertical stress of 0.5 MPa. As shown in the Eqs. (14), if the eroded particles move at a steady speed, then the slope in the double logarithmic coordinate system of TMSD will be 2; and when it acts under a steady fluid force, the corresponding slope is 4.

$$\begin{aligned} &\textbf{Constant } v\textbf{:}\quad \text{Distance} = v\cdot t \quad \text{TMSD} \sim t^2 \\ &\textbf{Constant } F\textbf{:}\quad \text{Distance} = \frac{F}{2m}t^2 \quad \text{TMSD} \sim t^4 \end{aligned} \tag{14}$$

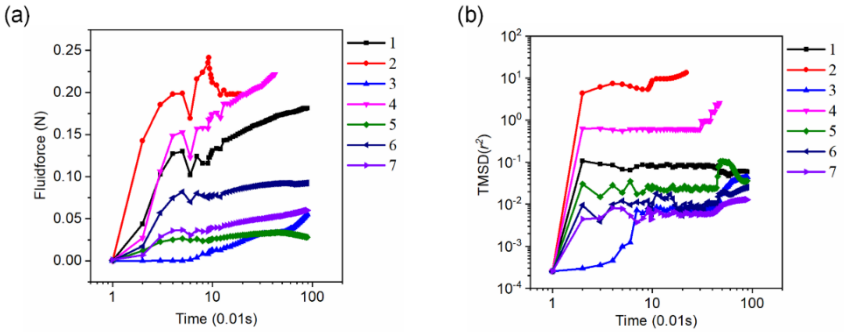

Fig. 2 (a) the variation of fluid force of eroded particles; (b) the TMSD of eroded particles; (I = 1.0, σ_v= 0.5MPa, horizontal flow)

In Figure 2b, the initial slope for the TMSD is larger than 4 in the log-log plot which means that eroded particles move under the action of an increasing fluid force of eroded particles, which is confirmed in Figure 2a.

To describe the particle sensitivity to fluid forces, the ratio between the mean contact force and fluid force of the eroded particles is judged by the following formula.

$$CR = \frac{\dfrac{1}{N_{\text{contact}}} \sum_{i=1}^{N_{\text{contact}}} \left\| \boldsymbol{F}_{\text{contact}} \right\|}{\left\| \boldsymbol{F}_{\text{fluid}} \right\|} \tag{15}$$

The development curve of CR in three typical particles are displayed in Figure 3. The particles transfer to non-contact when CR = 0. While an increase in CR means an increase in contact force or a decrease in fluid force, and the movability of the particles decreases accordingly. The process of monotonous descent in Fig. 3a corresponds to the particle keep moving continuously without encountering local blockage, especially in the progression of the initial steep drop. Figure 3(b)(c) corresponds to the typical behavior of particles trapped in a local pore structure, as the particles lose and gain contacts for several times. Overall, the general decrease in CR index in Figure 3 illustrates that the fluid force gradually dominates the competition with contact force and without any change in the stress boundary conditions, eroded particles do not get involved in the load-bearing skeleton anymore.

Based on the judgment between the direction of the fluid force and the direction of the contact force, a sliding index P of each contact pair of eroded particles is then proposed to determine whether the contact is going to slide or strengthen under the action of the fluid. The index P of a simple contact i can be computed according to the formula below,

$$P^{(i)}(\mathbf{m}) = \frac{1}{\tan\varphi^{(i)}} \frac{\left\| \mathbf{F}_{\text{t}}^{(i)} \right\|}{\left\| \mathbf{F}_{\text{m}}^{(i)} \right\|} \left[\frac{k_{\text{m}}^{(i)} \mathbf{m} \cdot \mathbf{m}_i}{\left\| \mathbf{F}_{\text{m}}^{(i)} \right\|} - \frac{k_{\text{t}}^{(i)} \mathbf{t}_i \cdot \mathbf{m}}{\left\| \mathbf{F}_{\text{t}}^{(i)} \right\|} \right] \tag{16}$$

where $\mathbf{m}$ is the direction of fluid force of a particle, $\mathbf{m}_i$ and $\mathbf{t}_i$ are the normal and tangential vector of the i-th contact of the particle; $\mathbf{F}_{\text{t}}^{(i)}$ and $\mathbf{F}_{\text{m}}^{(i)}$ are the tangential force and contact force

of *i*-th contact pair, $k_{\mathrm{m}}^{(i)}$ and $k_{\mathrm{t}}^{(i)}$ are the stiffness in the normal and tangential direction, $\varphi^{(i)}$ is the friction angle of *i*-th contact pair.

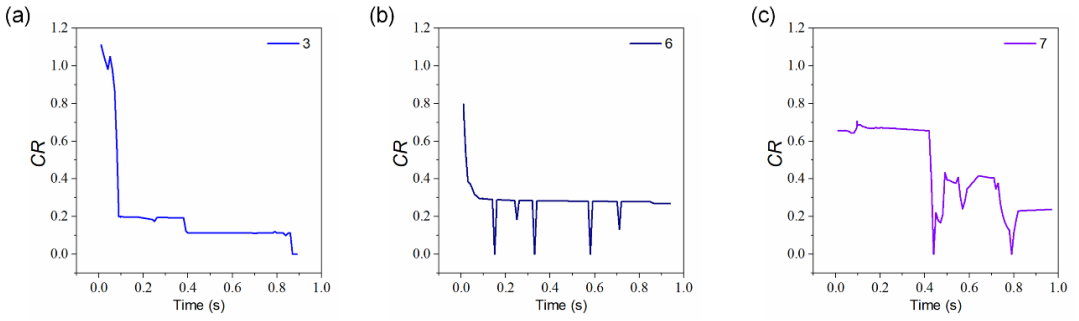

Fig. 3 Three typical *CR* evolution curves of eroded particles

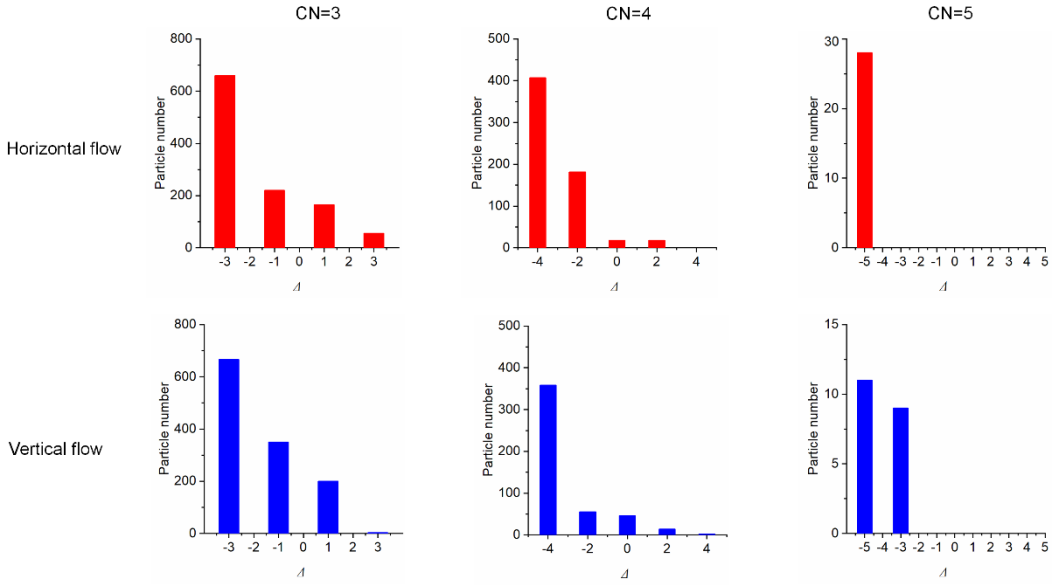

Fig.4 Distribution of Δ considering different CN and flow direction

According to the definition, $P<0$ reflects that the contact pair is going to slide and open if a fluid force in direction **m** is applied to the considered particle. $P^{(i)}$ index is attached to a given contact *i*. In order to construct a detachment index for a particle we define $\Delta=\mathrm{Number}(P^{(i)}(\mathbf{m})>0)-\mathrm{Number}(P^{(i)}(\mathbf{m})<0)$ which correspond to the difference between the number of contacts reinforced and weakened under the action of a fluid force in direction **m**. As a result, a negative value for Δ is proposed to characterize the overall detachment sensitivity of a given particle subjected to a fluid force in direction **m**.

Figure 4 shows the Δ distribution for the eroded particles with different contact number (CN) at critical time (i.e. when the particles are about to lose contact and become free particles). The distribution of Δ for the contacts of eroded particles just prior to their detachment well reflects the sliding tendency of contact pairs, because of the large proportion of negative value. Detached particles are thus characterized by a set of contact forces which are unable to balance the additional force applied by the fluid without sliding or opening.

4 CONCLUSIONS AND OUTLOOK

This paper adopted a three-dimensional coupled LBM-DEM method to simulate the phenomenon of suffusion considering anisotropy stress state. The microscale detachment mechanism is investigated by proposed sliding index and contact force ratio in horizontal and vertical flow conditions. The main conclusions can be summarized as follows:

- The initial steep slope of mean squared displacement of eroded grains is observed, which attributed to the continuous increase of fluid force. Regardless of the initial state, the ratio between the fluid force and the contact force of the eroded particles displays a downward trend over time, reflecting the gradual dominance of the fluid force, which eventually leads to particle detachment and erosion.
- Based on the judgment between the direction of the fluid force and the direction of the contact force, a contact sliding index P is then proposed to determine whether the contact is going to slide or strengthen under the action of the fluid. The distribution of P for the contacts of eroded particles just prior to their detachment reflects that fluid-induced sliding dominates.

The future work will be the evolution behavior of the force chain in the process of suffusion in different directions, and the characteristics of detached particles will be discussed from the perspective of the evolution of the stress distribution of fine particles to the whole sample; the fine particles will be introduced into a multi-scale model H-model, and the multi-scale constitutive model considering internal erosion will established. This part of work is already in progress.

REFERENCES

[1] M. Foster, R. Fell, M. Spannagle, The statistics of embankment dam failures and accidents, Can. Geotech. J. 37 (2000) 1000–1024.

[2] M. Foster, R. Fell, M. Spannagle, A method for assessing the relative likelihood of failure of embankment dams by piping, Can. Geotech. J. (2000). doi:10.1139/t00-029.

[3] A.W. Skempton, J.M. Brogan, Experiments on piping in sandy gravels, Geotechnique. 44 (1994) 449–460.

[4] M. Li, R.J. Fannin, Comparison of two criteria for internal stability of granular soil, Can. Geotech. J. 45 (2008) 1303–1309. doi:10.1139/T08-046.

[5] C. Chen, L.M. Zhang, D.S. Chang, Stress-Strain Behavior of Granular Soils Subjected to Internal Erosion, J. Geotech. Geoenvironmental Eng. (2016). doi:10.1061/(ASCE)GT.1943-5606.0001561.

[6] D. Marot, A. Rochim, H.H. Nguyen, F. Bendahmane, L. Sibille, Assessing the susceptibility of gap-graded soils to internal erosion: proposition of a new experimental methodology, Nat. Hazards. 83 (2016). doi:10.1007/s11069-016-2319-8.

[7] L. Ke, A. Takahashi, Experimental investigations on suffusion characteristics and its mechanical consequences on saturated cohesionless soil, Soils Found. (2014). doi:10.1016/j.sandf.2014.06.024.

[8] M. Xiao, N. Shwiyhat, Experimental investigation of the effects of suffusion on physical and geomechanic characteristics of sandy soils, Geotech. Test. J. (2012). doi:10.1520/GTJ104594.

[9] A. Mehdizadeh, M.M. Disfani, R. Evans, A. Arulrajah, Impact of suffusion on the cyclic and post-cyclic behaviour of an internally unstable soil, Geotech. Lett. (2019). doi:10.1680/jgele.18.00128.
[10] P.A. Cundall, O.D.L. Strack, A discrete numerical model for granular assemblies, Geotechnique. (1979). doi:10.1680/geot.1979.29.1.47.
[11] C. Kloss, C. Goniva, A. Hager, S. Amberger, S. Pirker, Models, algorithms and validation for opensource DEM and CFD–DEM, Prog. Comput. Fluid Dyn. an Int. J. 12 (2012) 140–152.
[12] J. Tao, H. Tao, Factors affecting piping erosion resistance: Revisited with a numerical modeling approach, Int. J. Geomech. (2017). doi:10.1061/(ASCE)GM.1943-5622.0000999.
[13] K. Kawano, T. Shire, C.O. Sullivan, Coupled particle-fluid simulations of the initiation of suffusion Coupled particle-fluid simulations of the initiation of suffusion, (2018). doi:10.1016/j.sandf.2018.05.008.
[14] J. Latt, O. Malaspinas, D. Kontaxakis, A. Parmigiani, D. Lagrava, F. Brogi, M. Ben Belgacem, Y. Thorimbert, S. Leclaire, S. Li, F. Marson, J. Lemus, C. Kotsalos, R. Conradin, C. Coreixas, R. Petkantchin, F. Raynaud, J. Beny, B. Chopard, Palabos: Parallel Lattice Boltzmann Solver, Comput. Math. with Appl. (2020). doi:10.1016/j.camwa.2020.03.022.
[15] D.R. Noble, J.R. Torczynski, A lattice-boltzmann method for partially saturated computational cells, Int. J. Mod. Phys. C. 9 (1998) 1189–1201. doi:10.1142/S0129183198001084.
[16] P.L. Bhatnagar, E.P. Gross, M. Krook, A model for collision processes in gases. I. Small amplitude processes in charged and neutral one-component systems, Phys. Rev. (1954). doi:10.1103/PhysRev.94.511.
[17] C.K. Aidun, J.R. Clausen, Lattice-Boltzmann Method for Complex Flows, Annu. Rev. Fluid Mech. (2010). doi:10.1146/annurev-fluid-121108-145519.
[18] S. Harris, An introduction to the theory of the Boltzmann equation, Courier Corporation, 2004.
[19] R.L. Liboff, Kinetic theory: classical, quantum, and relativistic descriptions, Springer Science & Business Media, 2003.
[20] D.R.J. Owen, C.R. Leonardi, Y.T. Feng, An efficient framework for fluid-structure interaction using the lattice Boltzmann method and immersed moving boundaries, Int. J. Numer. Methods Eng. (2011). doi:10.1002/nme.2985.
[21] T. Shire, C. O'Sullivan, K.J. Hanley, R.J. Fannin, Fabric and Effective Stress Distribution in Internally Unstable Soils, J. Geotech. Geoenvironmental Eng. 140 (2014) 04014072. doi:10.1061/(ASCE)GT.1943-5606.0001184.